

Adam PIORKOWSKI¹, Karolina NURZYNSKA², Cezary BOLDAK³, Daniel RESKA³,
Jolanta GRONKOWSKA-SERAFIN^{4,5}

SELECTED ASPECTS OF CORNEAL ENDOTHELIAL SEGMENTATION QUALITY

The number and shape of cells in endothelium layer is highly correlated with the quality of vision. Therefore, its precise and automatic description plays an important role in medicine.

This work presents several aspects of image processing of endothelium layer acquired by specular microscope. The comparison of cell selection accuracy is discussed using two different approaches to solve this problem: convolution filtering methods, and snake-based method. Moreover, for verification results generated by dedicated software, supplied with the microscope, were utilized. Next, the precise segmentation method is applied to improve the segmentation. The results are inspected visually, but also CV, H, and CVSL parameters, used in medicine, are calculated.

The research concludes that general visual outcomes achieved by all segmentation approaches give similar results, however deep insight into cell outline position reveals some differences, which were partially removed after precise segmentation application. The analysis of parameter values show high stability of CV and CVSL parameters.

1. INTRODUCTION

The human cornea is a very complex organ consisting of five layers: outer epithelium, Bowmans membrane, stroma, Descemets membrane and inner endothelium. Their cooperation is responsible for the quality of vision. However, any changes in a cornea, the translucent frontal part of the eyeball consisting of mainly parallel configuration of stromal fibers, influence considerably the refractive power of the human eye. Because it is the optical window of the eye, its transparency is crucial for proper organ functioning.

The corneal endothelium is a monolayer of hexagonal cells covering the posterior corneal surface, which removes the water that flows freely into the corneal structure from the anterior chamber and stabilise the corneal hydration at the level of 78%, thus assuring the transparency. Since the corneal endothelial cells do not reproduce their number decreases during the lifetime from 6500 cells/mm² at the birth to 1700 – 2000 cells/mm² at the age of 80 [14], [15]. Moreover, surgeries taking place in the anterior chamber, for instance the cataract or glaucoma

¹ AGH University of Science and Technology, Department of Geoinformatics and Applied Computer Science, Cracow, Poland

² Silesian University of Technology, Institute of Informatics, Gliwice, Poland

³ Bialystok University of Technology, Bialystok, Poland

⁴ Oejenafdelingen, Regionshospitalet Holstebro, Laegaardvej 12a, 7500 Holstebro, Denmark

⁵ Pomeranian Medical University, Department of Ophthalmology, Szczecin, Poland

surgery, are responsible for additional cell number diminishing which may elevate within a months after the surgery. Similarly other conditions, like trauma, inflammation, elevated intraocular pressure or some diseases (e.g. diabetes), influence the cell loss. When the density decreases below 1000 cells/mm^2 the cornea has no possibility to dehydrate and the endothelial insufficiency occurs, which leads to irreversible corneal edema responsible for severe vision loss [10]. In consequence of the tight structure of this layer, the enlargement and changes of original hexagonal shape of cells, due to filling in the region that has remained after the necrotic cell, are noticeable. Therefore, the deviation in cell shape indicates the corneal damage.

Specular microscopy allows to assess the endothelial layer in vivo. In this work Topcon SP1000 noncontact specular microscope was applied for data acquisition from several subjects. The images presenting the corneal endothelium structure are stored at 8-bits gray-scale color depth with resolution around 200×450 pixels.

The goal of the image processing is to define with the highest accuracy the borders of the endothelium cells, which enable shape parameter calculation and in consequence corneal medical state description. It is non-trivial task due to the acquisition noises, irregular lighting illumination, and low contrast of the data. There are several solution already presented in the literature, e. g. [3], [6], [8], [9], however its comparison is unknown to the authors. Therefore, the main interest of this work is the comparison of accuracy of two chosen techniques for endothelium cells segmentation, which is done visually and by the means of dedicated parameters calculation. Moreover, some improvements for methods based on active contours described in [3] are suggested and also all results are processed by precision improving algorithm designed in [22], which is also a novel approach.

2. CELL SEGMENTATION

This problem of cell segmentation exists in the research domain and some solution have been already presented. First approaches based mostly on pyramid methods used for image processing [1] or the convolution kernels, which differ in proposed masks [16], [18]. These solutions are very inaccurate in case of irregular lighting therefore when applied need additional preprocessing. Nadachi and Nunokawa [17] developed a scissoring operator that separates the cells into the binary image, where the standard solution is to use a kind of watershed algorithm. Next, in the work [28] the scale-space filtering was suggested using the Gaussian kernels and a variant of unsharp masking. More recently, the non-sampled Wavelet pyramid decomposition of low pass regions was exploited [13] followed by thinning the boundaries. In [30] several binarization approaches are described.

This research investigates the accuracy of cell segmentation when different algorithms are applied. Due to the lack of space only two exemplary solutions are presented. First of them bases on convolution kernels, whereas the second uses active contours. Details of each method are given below.

2.1. SEGMENTATION WITH CONVOLUTION KERNELS

Segmentation based on convolution kernels demands following several steps of image processing before the result is achieved as depicted in Fig. 1. The preprocessing assumes noise and artifacts removal with special care for lighting improvement. The method exploits morphological convolution filtering for noise removal followed by lighting normalization described in [8]. The authors notice that the illumination changes in a column-wise manner, therefore they average the columns illuminance, which proved to give good performance.

Then the binarization procedure is applied, which divides the image into the background

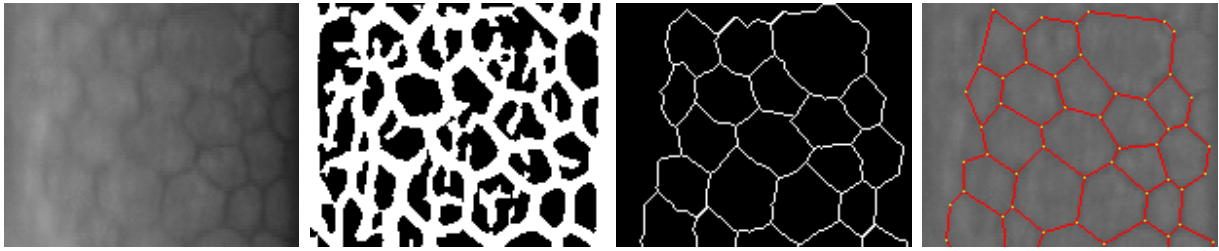


Fig. 1. Cell segmentation using KH algorithm. From the left: original image, binarization resulting from KH algorithm application, skeletonization achieved after application of iterative morphological thinning with mask A, and incorporation of the cell boundaries on the original image.

(0 values) and objects (denoted with label value 1). There are many possible rules for the mapping definition. The simplest one assumes using a threshold value basing on the image intensity levels. Yet, this solution is imperfect and prone to irregular illumination and noise in the data. Hence, more sophisticated approaches are necessary to enable accurate binarization in case of the corneal endothelium processing. One can take into consideration watershed algorithm, adaptive binarization [30], filter based binarization [30] and its improved versions [21]. Yet, the best results are achieved with KH approach which was exploited in presented research.

KH algorithm, presented in [8], is another promising approach to endothelium cell binarization. It demands preliminary image preprocessing in order to noise removal, then each one of four directional masks of resolution 9×9 is exploited to find partial binarization followed by small object removal. Finally, the resulting masks are summed and negated to prepare the final outcome.

Nevertheless which method was applied for binarization of the image, the outcome results in thick boundaries of the cells. Since the most interesting is the area of each cell and its side lengths, it should be possible to appoint these parameters unequivocally, hence skeletonization of the boundaries is necessary. There are several methods to fulfill this task, which summary might be found in [27]. However, authors in [22] decided to use the iterative approach using morphological operators with 3×3 masks designing the precise segmentation method.

2.2. APPROACH BASED ON MULTIPLE MERGING ACTIVE CONTOURS

This method segments the hexagonal cells with multiple active contours [12], evolving concurrently and not overlapping. It is an evolution following the ideas from [3] and reformulating some energies, incorporating more advanced image preprocessing, introducing the snake ability to merge with a neighbor if they both were initialized inside a single cell and other extensions. The implementation has been done using the MESA platform [26].

Method outline. The proposed algorithm is composed of the four steps:

- image preprocessing,
- binarization,
- initial detection of the cell bodies,
- active contour segmentation of the cell contours.

All of them are automatic and do not require an operator interaction. Each step is described in details below.

To decrease the parameter number we introduce one meta-parameter – *scale*, characterizing the image spatial resolution. Its value is set proportionally to the mean cells diameter in the image with the value 1 corresponding to 15 pixels. Several further parameters are defined in function of *scale*.

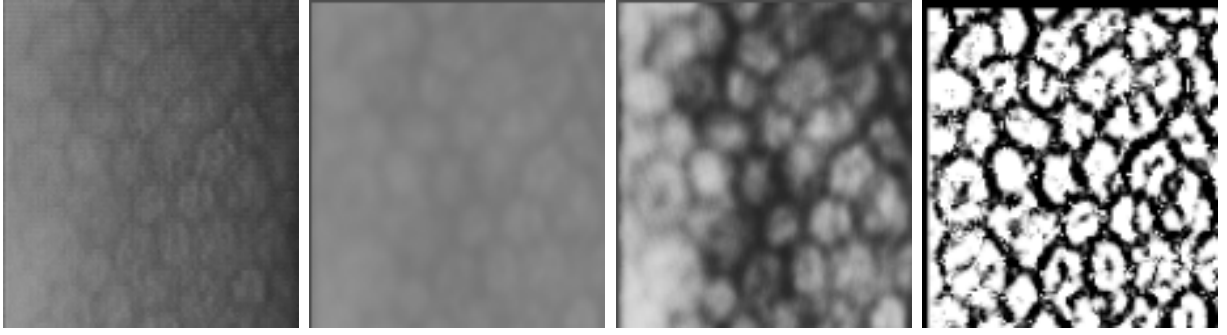


Fig. 2. Preprocessing steps before the active contour method application. From the left: exemplary image, illumination correction, result of histogram equalization, and result of the line filtering.

Image preprocessing. As it is common in many real image processing techniques, especially in case of the biomedical data, the input image is filtered with the *Gauss low-pass convolution filter* with the standard deviation $\sigma = 1.5 \cdot scale$. The analyzed images are very often unequally illuminated. To fix this artifact, from the original image one subtracts its Gauss filtered version with $\sigma = 30$ (Fig. 2). The offset 127 is applied to avoid negative values. The last step applies the histogram equalization procedure to uniformly distribute the intensity levels (Fig. 2).

Additional preprocessing is performed but its result is not used during the full segmentation workflow. It is stored only for the contour merging step (see below). This preprocessing consists of a line filtering using the Hessian eigenvalues. Computed locally for every pixel, the eigenvalues λ_1 and λ_2 define the filter output:

$$\frac{\lambda_1}{1 + |\lambda_2|}, \quad (1)$$

after rejecting the negative values, negating and scaling (Fig. 2).

Binarization and initial detection of the cell bodies. These two steps are performed exactly as in [3]. The adaptive thresholding is employed to separate the cell bodies from the space between them: local thresholds are computed as the local intensity means incremented by some small constant value. The initial cell bodies (input to the final segmentation) are detected as maximum circles located inside the thresholded cell areas. Some of them are then merged if their final form fits inside this area to take into account more elongated cell shapes.

Multiple merging active contours. The initial approximation of the cell bodies is then deformed to fit the actual cell shapes with the technique of *active contours – snake* [12]. Its discrete version is used here where the evolving curve is represented by the collection of points (with integer coordinates) given the local energy. The MESA snake model [26] is composed of several snakes separated spatially and evolving concurrently. In each iteration a better location of each snaxel is looked for, minimizing its local energy. After each iteration several MESA extensions are fired, manipulating the contour form.

The local energy of the snaxel p_i (or its new examining position) of the contour j is the weighted sum of four composing MESA energies:

$$E(p_i^j) = \omega_{im} E_{image}(p_i^j) + \omega_{sm} E_{smoothness}(p_i^j) + \omega_{reg} E_{regularity}(p_i^j) + \omega_{bal} E_{balloon}(p_i^j). \quad (2)$$

- 1) *Image energy* for each snaxel is the mean intensity along two lines going to the neighbor snaxels (previous and next ones). In comparison to the previous version (intensities taken only at the snaxel position) this approach better places the contour, taking into account the complete contour form, not only the snaxel positions.

$$E_{image}(p_i^j) = \frac{1}{|P_i^j|} \sum_{p \in P_i^j} I(p), \quad (3)$$

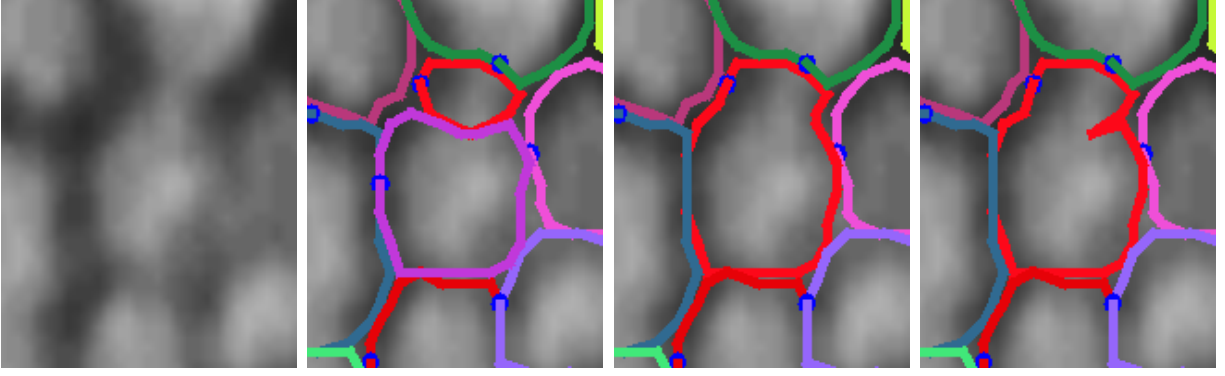


Fig. 3. Merging the neighbor snakes. From the left: original image, contours before merging, merged contours (spike detection), merged contours (no spike detection).

where P_i^j – set of points (pixels) on segments $p_{i-1}^j - p_i^j$ and $p_i^j - p_{i+1}^j$ given by the Bresenham algorithm.

- 2) *Smoothness energy* taken directly from [3]:

$$E_{smoothness}(p_i^j) = \left| \frac{v_{prev}}{|v_{prev}|} + \frac{v_{next}}{|v_{next}|} \right|, \quad (4)$$

where v_{prev} and v_{next} – vectors going from p_i^j to p_{i-1}^j and p_{i+1}^j .

- 3) *Regularity energy* also taken from [3]:

$$E_{regularity}(p_i^j) = \frac{(avg^j - |v_{prev}|)^2 + (avg^j - |v_{next}|)^2}{(avg^j)^2}, \quad (5)$$

where avg^j – the mean inter-snaxel distance in the contour j .

- 4) *Balloon energy* reformulated to become the regular energy (being a force in [3]) – the negative scalar product of two vectors: (1) v_center_j going from the geometrical center c^j of the contour j to the old snaxel position (from previous iteration) – $old_p_i^j$ and (2) $v_evolution_i^j$ going from $old_p_i^j$ to p_i^j (after making them unit ones).

$$E_{balloon}(p_i^j) = -\mu \frac{v_center_j}{|v_center_j|} \cdot \frac{v_evolution_i^j}{|v_evolution_i^j|}. \quad (6)$$

Because the choice of influence (weight) of this energy can be crucial to the correct border delimitation (too low stops the evolution before reaching the target, too high makes the contour to overpass it) we introduce the multiplying factor μ . It is initialized with low value and doubled each time no contour expansion is observed (they are forbidden to shrink). This formula: (1) promotes evolution toward the outside of the contour, (2) assures reaching the cell borders in the same time even if the contours are initialized in different distance from them, (3) expands the contours to all regions in the image.

The MESA extensions manipulate the contour shapes between the iterations by:

- 1) *Border snake merger* merges two neighbor contours if their touching fragments are located (in greater part) in the “valley”: points that have the line filter response below value 100 (Eq. 1, Fig. 2). The limit is put on the result merged shape in terms of size and aspect ratio. The effects are presented in Fig. 3.
- 2) *Spike remover* during the merging process sometimes the common fragment detected is too short, forming sharp spikes in the new merged shape. This extension detects such points with too close vectors going to neighbor snaxels and removes them (Fig. 3).
- 3) *Point remover* removing one of two snaxels if they are too close to each other.

- 4) *Point adder* adding an extra snaxels between too distant two snaxles.
- 5) *Small snake remover* removes too small snakes. This gives an opportunity to the neighbor contours to take the freed space.

3. PRECISION OF SEGMENTATION

The accuracy in determining the cells boundaries is very important (e.g. [11]), as the movement of one vertex joining edges of adjacent cells changes the shape and area of all cells in its neighborhood. Therefore, authors in [22] proposed an precise segmentation method which solves this problem using two step algorithm. Firstly the neighborhood map is prepared which selects the number of neighbors with brightness values in the source image above the input pixel value. In result small values in the map correspond to the cells and higher values depict the valleys. Secondly the modified thinning algorithm is applied, which performs several classical iterations, however each time values from the map, which value corresponds to current iteration number, undergo skeletonization procedure. The original algorithm enables the choice of one of three masks, however in this research we had concentrated on mask A.

Although the proposed method can be applied to precise segmentation of binary images, it can be used for lines already carried out by any segmentation algorithm. To improve borders, firstly a dilatation is made, and next the full precise segmentation can be performed.

4. PARAMETERS

As was mentioned in the Introduction, the changes in the corneal endothelium are correlated to the shape variation of the cells incorporated in this layer. In this work following parameters are investigated to give better insight in compared image processing methodologies:

H Hexagonality [5] – percentage of hexagonal cells

$$H = \frac{N_6}{N_T} \cdot 100\%, \quad (7)$$

where N_6 is the number of six-side cells and N_T is the total number of cells in the image.

CV Coefficient of Variations in area size of different cells [4]

$$CV = \frac{1}{\mu_c} \sqrt{\frac{1}{N} \sum_{i=1}^N (c_i - \mu_c)^2}, \quad (8)$$

where c_i is the area of i th cell and μ_c is the average are of cells in the image.

CVSL Average Coefficient of Variation of the cell Sides Lengths [7]

$$CVSL = \frac{1}{N} \sum_{j=1}^N \frac{1}{\mu_{SL}} \sqrt{\frac{1}{N_L} \sum_{i=1}^{N_L} (l_i - \mu_{SL})^2}, \quad (9)$$

where l_i is the length of the i th side of the j th cell , μ_{SL} is the average length of the all sides of j th cell and N_L is the number of sides and N the number of cells.

5. RESULTS AND DISCUSSION

The aim of the presented experiment is to compare the precision of endothelium cell segmentation by two methods, characterized by different approaches, and verified with a dedicated

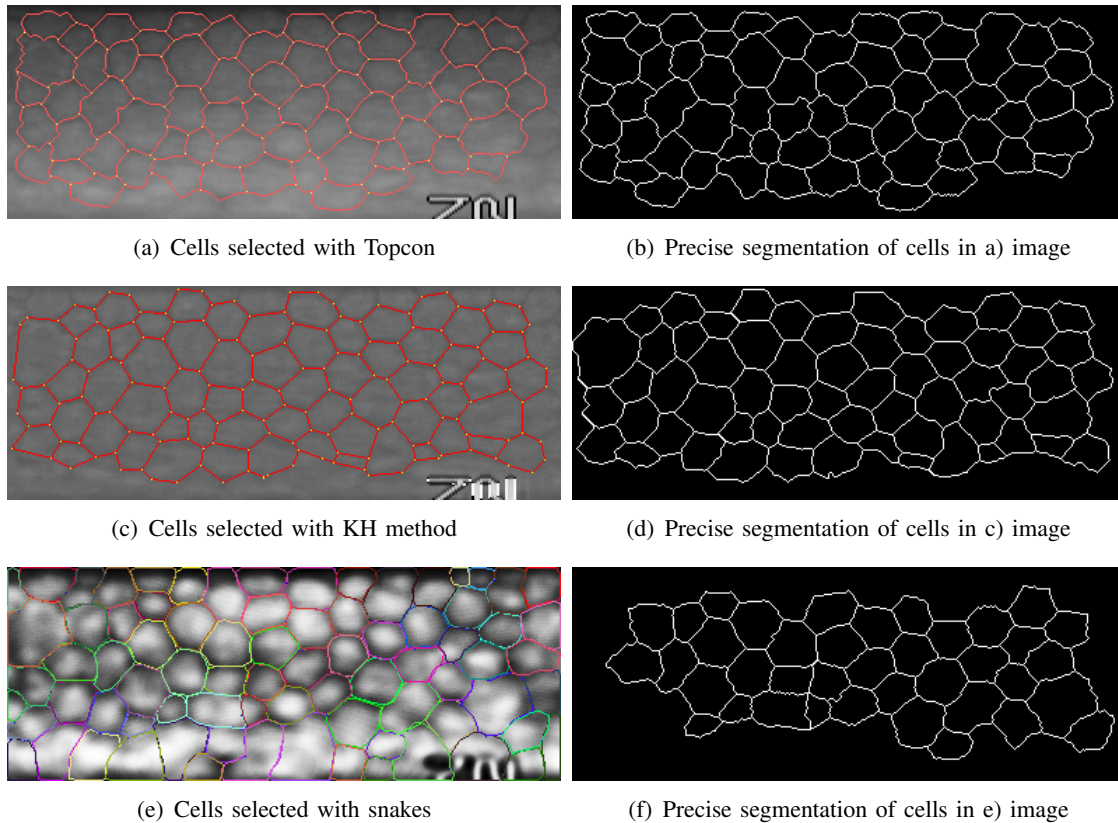


Fig. 4. Comparison of endothelium cell segmentation with Topcon software (top row), KH method (middle row) and snake approach (bottom row) with additional visualization of cell borders accuracy after application of precise segmentation algorithm (right column).

software for Topcon microscope. Figure 4. (left column) presents results generated by each method. From the global point of view, all algorithms found the cells and looks similar. However, in the case of snake approach the cells close to the image border are influenced by it and must be removed for further processing. When examining precisely by following the position of each cell edge, one can see the differences of presented approaches. On this stage however, it is difficult to state which solution gives better outcome. Next, Fig. 4. (right column) shows the data additionally processed by precise segmentation method, which moved the edges closer to the valleys between cells, thus making the achieved results even more similar.

For medical purposes visual inspection is insufficient, therefore several parameters are derived to describe the endothelium cells quality. Table 1 collects the parameters calculated for the data depicted in Fig. 4. The CVSL parameter seems to be very stable and takes similar values, except the case of KH method, when some cells on the left change their shape which influences the results. It is due to the fact that this parameter is sensitive to stretching of the object outline. The H parameter does not convey any information about data changes. Generally, it is known that this measure is unstable and result in high variations for small data changes [23]. The CV parameter values presented the higher variability depending on the chosen cell segmentation method, moreover incorporating the precise segmentation did not influenced the results considerably. Most likely it is due to the variability in cell edge definition in each method, however it is worth to point out that the count of the cells might vary slightly (by up to 5 elements). Finally, application of the precise segmentation method did not influence the results, except the KH method, where it resulted in reduction of two cells.

Table 1. Parameters calculated for the exemplary data presented in Fig. 4.

Method	CVSL	H	CV
Topcon	0.2505	58	0.3090
Topcon + prec seg	0.2544	58	0.3100
KH	0.2618	57	0.3570
KH + prec seg	0.2487	61	0.3450
Snake	0.2675	58	0.3140
Snake + prec seg	0.2639	53	0.3230

6. CONCLUSIONS

This work compares methods presenting two different approaches for endothelium cell segmentation with additional verification by data gathered from the dedicated software for Topcon microscope. The visual inspection of achieved cell boundary detection shows good quality of each method. Next, application of precise segmentation approach presented small improvement in cell outline description. Final comparison by parameters used in medicine proved stability of compared solutions.

In future research, new criterion of data description quality are going to be derived. Moreover the cell segmentation by other method should be investigated. The most promising methods seem to be the algorithms presented in [25], which exploits a classifier based on several cell shape parameters to find the borders and the one using spatial frequency analysis described in [29]. Although, both solutions still need a manual cell count or manual corrections. The intelligent methods such as neural networks or the rough sets [24], [19], [20], [2] are also taken into account.

ACKNOWLEDGEMENT

This work was financed by the AGH - University of Science and Technology, Faculty of Geology, Geophysics and Environmental Protection as a part of statutory project. C. Boldak and D. Reska were supported by the grants S/WI/2/2013 and W/WI/5/2014 from Bialystok University of Technology.

BIBLIOGRAPHY

- [1] ADELSON E. H., ANDERSON C. H., BERGEN J. R., BURT P. J., OGDEN J. M. Pyramid methods in image processing. RCA engineer, 1984, Vol. 29. pp. 33–41.
- [2] BIELECKA M., BIELECKI A., KORKOSZ M., SKOMOROWSKI M., WOJCIECHOWSKI W., ZIELINSKI B. Application of shape description methodology to hand radiographs interpretation. Computer Vision and Graphics, 2010, Vol. 6374 of Lecture Notes in Computer Science. Springer, pp. 11–18.
- [3] CHARLAMPOWICZ K., RESKA D., BOLDAK C. Automatic segmentation of corneal endothelial cells using active contours. Advances In Computer Science Research, 2014, Vol. 14. pp. 47–60.
- [4] DOUGHTY M. The ambiguous coefficient of variation: Polymegethism of the corneal endothelium and central corneal thickness. International Contact Lens Clinic, 1990, Vol. 17. pp. 240–248.
- [5] DOUGHTY M. Concerning the symmetry of the hexagonal cells of the corneal endothelium. Experimental eye research, 1992, Vol. 55. pp. 145–154.
- [6] FORACCHIA M., RUGGERI A. Corneal endothelium analysis by means of bayesian shape modeling. Proc. 25th Annual International Conference of the IEEE-EMBS, 2003. pp. 794–797.
- [7] GRONKOWSKA-SERAFIN J., PIORKOWSKI A. Corneal endothelial grid structure factor based on coefficient of variation of the cell sides lengths. Image Processing and Communications Challenges 5, 2014, Vol. 233 of Advances in Intelligent Systems and Computing. Springer, pp. 13–19.
- [8] HABRAT K. Binarization of corneal endothelial digital images. 2012.
- [9] HABRAT K., HABRAT M., GRONKOWSKA-SERAFIN J., PIORKOWSKI A. Cell detection in corneal endothelial images using directional filters. Image Processing and Communications Challenges 7, 2016, Vol. 389 of Advances in Intelligent Systems and Computing. Springer.

- [10] HOPPENREIJS V., PELS E., VRENSSEN G., TREFFERS W. Corneal endothelium and growth factors. *Survey of Ophthalmology*, 1996, Vol. 41. Elsevier, pp. 155–164.
- [11] JAWOREK-KORJAKOWSKA J., TADEUSIEWICZ R. Determination of border irregularity in dermoscopic color images of pigmented skin lesions. *Engineering in Medicine and Biology Society (EMBC), 2014 36th Annual International Conference of the IEEE*, 2014. pp. 6459–6462.
- [12] KASS M., WITKIN A., TERZOPOULOS D. Snakes: Active contour models. *International Journal of Computer Vision*, 1988, Vol. 1. pp. 321–331.
- [13] KHAN M. A. U., NIAZI M. K. K., KHAN M. A., IBRAHIM M. T. Endothelial cell image enhancement using non-subsampled image pyramid. *Information Technology Journal*, 2007, Vol. 6. pp. 1057–1062.
- [14] KO M., LEE J., CHI J. Cell density of the corneal endothelium in human fetus by flat preparation. *Cornea*, 2000, Vol. 19. pp. 80–83.
- [15] KO M., PARK W., LEE J., CHI J. A histomorphometric study of corneal endothelial cells in normal human foetuses. *Exp Eye Res*, 2001, Vol. 72. pp. 403–409.
- [16] MAHZOUN M., OKAZAKI K., MITSUMOTO H., KAWAI H., SATO Y., TAMURA S., KANI K. Detection and complement of hexagonal borders in corneal endothelial cell image. *Medical Imaging Technology*, 1996, Vol. 14. pp. 56–69.
- [17] NADACHI R., NUNOKAWA K. Automated corneal endothelial cell analysis. *Computer-Based Medical Systems, 1992. Proceedings., Fifth Annual IEEE Symposium on*, 1992. pp. 450–457.
- [18] OBLAK E., DOUGHTY M., OBLAK L. A semi-automated assessment of cell size and shape in monolayers, with optional adjustment for the cell-cell border width-application to human corneal endothelium. *Tissue and Cell*, 2002, Vol. 34. pp. 283–295.
- [19] OGIELA M., TADEUSIEWICZ R. Artificial intelligence methods in shape feature analysis of selected organs in medical images. *Image Processing and Communications*, 2000, Vol. 6. pp. 3–11.
- [20] OSZUTOWSKA-MAZUREK D., MAZUREK P., SYCZ K., WAKER-WÓJCIUK G. Estimation of fractal dimension according to optical density of cell nuclei in papanicolaou smears. *Information Technologies in Biomedicine*, 2012. Springer, pp. 456–463.
- [21] PIORKOWSKI A., GRONKOWSKA-SERAFIN J. Selected issues of corneal endothelial image segmentation. *Journal of Medical Informatics & Technologies*, 2011, Vol. 17. pp. 239–245.
- [22] PIORKOWSKI A., GRONKOWSKA-SERAFIN J. Towards precise segmentation of corneal endothelial cells. *Bioinformatics and Biomedical Engineering*, 2015, Vol. 9043 of Lecture Notes in Computer Science. Springer International Publishing, pp. 240–249.
- [23] PIORKOWSKI A., MAZUREK P., GRONKOWSKA-SERAFIN J. Comparison of assessment regularity methods dedicated to isotropic cells structures analysis. *Image Processing and Communications Challenges 6*, 2015, Vol. 313 of Advances in Intelligent Systems and Computing. Springer, pp. 169–178.
- [24] PLACZEK B. Rough sets in identification of cellular automata for medical image processing. *Journal of Medical Informatics and Technologies* (ISSN: 1642-6037), 2013, Vol. 22. pp. 161–168.
- [25] POLETTI E., RUGGERI A. Segmentation of corneal endothelial cells contour through classification of individual component signatures. *XIII Mediterranean Conference on Medical and Biological Engineering and Computing 2013*, 2014. pp. 411–414.
- [26] RESKA D., JURCZUK K., BOLDAK C., KRETOWSKI M. Mesa: Complete approach for design and evaluation of segmentation methods using real and simulated tomographic images. *Biocybernetics and Biomedical Engineering*, 2014, Vol. 34. pp. 146–158.
- [27] SAEED K., TABĘDZKI M., RYBNIK M., ADAMSKI M. K3M: A universal algorithm for image skeletonization and a review of thinning techniques. *International Journal of Applied Mathematics and Computer Science*, 2010, Vol. 20. pp. 317–335.
- [28] SANCHEZ-MARIN F. Automatic segmentation of contours of corneal cells. *Computers in Biology and Medicine*, 1999, Vol. 29. pp. 243–258.
- [29] SELIG B., VERMEER K. A., RIEGER B., HILLENAAR T., HENDRIKS C. L. L. Fully automatic evaluation of the corneal endothelium from in vivo confocal microscopy. *BMC Medical Imaging*, 2015, Vol. 15. BioMed Central Ltd, p. 13.
- [30] SZOSTEK K., GRONKOWSKA-SERAFIN J., PIORKOWSKI A. Problems of corneal endothelial image binarization. *Schedae Informaticae*, 2011, Vol. 20. pp. 211–218.

